



CHORUS

This is the accepted manuscript made available via CHORUS. The article has been published as:

Interface roughness governed negative magnetoresistances in two-dimensional electron gases in AlGaN/GaN heterostructures

Ting-Ting Wang, Sining Dong, Zhi-Li Xiao, Chong Li, Wen-Cheng Yue, Bin-Xi Liang, Fei-Fan Xu, Yong-Lei Wang, Sheng-Rui Xu, Xiao-Li Lu, Jianhua Li, Chenguang Wang, Zixiong Yuan, Song-Lin Li, Guo-Zhu Sun, Bin Liu, Hai Lu, Hua-Bing Wang, and Wai-Kwong Kwok

Phys. Rev. Materials **5**, 064003 — Published 10 June 2021

DOI: [10.1103/PhysRevMaterials.5.064003](https://doi.org/10.1103/PhysRevMaterials.5.064003)

Interface roughness governed negative magnetoresistances in two-dimensional electron gases in AlGaN/GaN heterostructures

Ting-Ting Wang¹, Sining Dong¹, Zhi-Li Xiao^{2,3,*}, Chong Li¹, Wen-Cheng Yue¹, Bin-Xi Liang¹, Fei-Fan Xu¹, Yong-Lei Wang^{1,*}, Sheng-Rui Xu⁴, Xiao-Li Lu^{4,*}, Jianhua Li¹, Chenguang Wang¹, Zixiong Yuan¹, Song-Lin Li¹, Guo-Zhu Sun^{1,5}, Bin Liu¹, Hai Lu¹, Hua-Bing Wang^{1,5}, and Wai-Kwong Kwok²

¹*School of Electronic Science and Engineering, Nanjing University, Nanjing, 210023, China*

²*Materials Science Division, Argonne National Laboratory, Argonne, IL 60439, USA*

³*Department of Physics, Northern Illinois University, DeKalb, IL 60115, USA*

⁴*School of Microelectronics & State Key Discipline Laboratory of Wide Bandgap Semiconductor Technology, Xidian University, Xi'an, 710071, China*

⁵*Purple Mountain Laboratories, Nanjing, 211111, China*

Negative magnetoresistances (NMRs) have been widely observed in two-dimensional electron gases (2DEGs). However, their origins are under debate. Here, we report on NMRs in the 2DEG in AlGaN/GaN heterostructures, aiming to uncover their origins by utilizing electric field gating. We systematically measured the magnetoresistances in magnetic fields up to 12 T and at temperatures between 3 K and 260 K and observed NMRs over a wide range of temperatures from 3 K to 170 K, which become more pronounced with decreasing temperature. We conducted electric field gating experiments to correlate the occurrence of NMRs with the relationship between electron mobility and density. The latter is governed by defect scattering sources in the sample and can be theoretically modelled. Comparison of the measured electron mobility and electron density relationship with theory reveals that interface roughness scattering plays a crucial role in obtaining large NMRs. Our work demonstrates that electric field gating provides a means not only to tune the values of NMRs but also to uncover their mechanisms.

I. INTRODUCTION

Negative magnetoresistances (NMR), where the magnetic field induces a decrease in the electrical resistance, is ubiquitous in two-dimensional electron gases (2DEGs) formed at the interfaces of various semiconductor heterostructures [1-23]. A common mechanism that can cause NMRs in 2DEGs is the weak localization (WL) of noninteracting electrons due to quantum interference effect [13-15,17-21]. The WL-induced NMRs only occur at low temperatures and at low magnetic fields, i.e., $\omega_c\tau < 1$ with ω_c being the cyclotron frequency and τ being the relaxation time. Their amplitudes are typically small ($< -1\%$) and saturate quickly with increasing magnetic field. They also exhibit characteristic cusps at zero field in the resistance versus magnetic field $R(B)$ curves and therefore can be identified without difficulties. On the other hand, NMRs in some 2DEGs can be as large as -92% [8] and persist up to very high magnetic fields where $\omega_c\tau \gg 1$ [19,22]. Various theories have been proposed to explain the underlying mechanisms that could lead to those large NMRs [24-31]. To date, the variety of non-WL NMRs observed in 2DEGs has been mostly attributed to electron–electron interaction (EEI) effect [1,2,24-26], Lorentz gas model [11,12,27,28], and memory effects resulting from the return events of an electron to a scatterer after a single collision process with another scatterer [19,29]. Recently, a theory [31] based on viscous flows of electrons could reproduce the colossal NMRs observed in 2DEGs in AlGaAs/GaAs heterostructures [8]. Besides a few experiments that are particularly designed to prove theoretical predictions [11,12], in many cases, the behavior of the temperature and field dependence of the magnetoresistance is used to reveal a proposed mechanism [1,2,19]. Conclusions attained this way can be indecisive, since similar NMR behaviors can originate from

different mechanisms. For example, NMRs originating from both EEI [2,26] and memory effects [29] exhibit parabolic magnetic field dependence. Furthermore, the observed NMRs may be a result of several combined mechanisms, thereby complicating the analysis of the experimental data [19]. Here, we show that additional information on the origins of NMRs in 2DEGs can be obtained by electric field gating investigations of the electron mobility versus density relationship that can directly reflect the scattering sources in the sample [32-35].

AlGa_N/Ga_N heterostructures have attracted extensive attention over the past years because they are well suited for fabricating high power and high frequency field effect transistors [36-38]. Good device performances hinge on the combination of their high carrier density and high breakdown fields [38]. The spontaneous and strong piezoelectric polarization in AlGa_N/Ga_N heterostructures [39-41] creates a triangular quantum well resulting in 2DEGs with densities reaching values of $\sim 10^{13}$ cm⁻², which is nearly two orders of magnitude larger than the typical densities ($\sim 10^{11}$ cm⁻²) of 2DEGs in AlGaAs/GaAs systems [6-8]. Here we do not study other remarkable properties of the AlGa_N/Ga_N heterostructure but focus on the origin of NMRs by taking advantage of the well-established relationship between the scattering sources and the density dependence of the electron mobility. The mobilities of the 2DEGs in AlGa_N/Ga_N heterostructures are very limited (up to 10^4 cm²V⁻¹s⁻¹). Thus, their mean free paths (see Fig.S1(b)) can be much smaller than the sample width, excluding mechanisms such as viscous flows [31] for the observed NMRs. The relationship between the scattering sources and the density dependence of the electron mobility, which can be obtained via electric field gating, has been extensively investigated both experimentally [32,33] and theoretically [see supplement]. That is, the scattering

source(s) causing the NMRs can be directly uncovered from the density dependence of the electron mobility. Here, we conduct a systematic investigation of electric field gating effect on the NMRs 2DEGs in AlGa_N/Ga_N heterostructures to identify the regime where NMRs are observed in the density dependence of the electron mobility, revealing the crucial role played by the interface roughness [42,43] on the occurrence of large NMRs. This work demonstrates that electric field gating provides a means not only to tune the values of NMRs but also to uncover their mechanisms. It also indicates that magnetotransport can be used to characterize large-angle interface roughness scattering in AlGa_N/Ga_N heterostructures.

II. EXPERIMENTAL METHODS

The AlGa_N/Ga_N heterostructures investigated in this work were grown by metal-organic chemical vapor deposition (MOCVD) on sapphire substrates. Their layer structure is illustrated by the schematic presented in Fig.1(a). An AlN barrier layer was added between the AlGa_N layer and the Ga_N buffer to reduce the alloy disorder scattering by minimizing the wave function penetration from the 2DEG channel into the AlGa_N layer [44]. The 2DEG is realized due to spontaneous and piezoelectric polarizations in the Ga_N layer near the Ga_N/AlN interface. The measured samples were fabricated from the AlGa_N/Ga_N heterostructure into a Hall bar geometry using photolithography, followed by inductively coupled plasma (ICP) etching. Ohmic contacts of Ti(20nm)/Al(120nm)/Ni(50nm)/Au(100 nm) were made by means of electron-beam evaporation (EBE), followed with a 30 s rapid thermal annealing at 850 ° C. Lastly, the gate electrode comprised of Ti(20 nm)/Au(100 nm) was made by means of EBE. Micrographs of a typical sample

(Sample W1) are presented in Fig.1(b).

We conducted conventional resistance measurements in an Oxford Instrument system (TeslatronPT) under constant current mode. Magnetic fields up to 12 Tesla were applied out-of-plane, i.e., perpendicular to the plane of the 2DEG. We define the magnetoresistance as $MR = (R - R_0)/R_0$, where R and R_0 are resistances at a fixed temperature with and without an applied magnetic field, respectively. We measured two samples (Sample W1 and Sample W2). Each of them has two sets of voltage contacts of neighboring sections (denoted as CH1 and CH2 in Fig.1(b) for Sample W1). Results from both CH1 and CH2 are nearly the same (see Fig.S1) [45]. We present results from CH1 of Sample W1 in the main text. Data from CH2 of Sample W1 and Sample W2 are presented in the supplement (see Fig.S1, Fig.S2 and Fig.S4) [45].

III. RESULTS AND DISCUSSION

Inset of Fig.1(c) exhibits $R_{xy}(B)$ curves obtained at the lowest ($T = 3$ K) and highest ($T = 260$ K) experimental temperatures. They indicate that the amplitude of the Hall resistances increases monotonically with increasing magnetic field and the slopes of $R_{xy}(B)$ curves are nearly independent of the temperature, which is the classical characteristic of Hall resistances for one type of charge carriers with a density that is temperature-insensitive. The slopes of the $R_{xy}(B)$ curves at various temperatures or the $R_{xy}(T)$ curve at a fixed magnetic field enables us to obtain the electron density. We measured $R_{xy}(T)$ at $B = 9$ T (see upper curve in Fig.1(c)) and obtained the temperature dependence of the electron density $n(T)$ as shown in Fig.1(d). The electron density is nearly temperature-independent, with values of $1.02 \times 10^{13}/\text{cm}^2$ at $T = 3$ K and $1.12 \times 10^{13}/\text{cm}^2$ at T

= 260 K, consistent with calculated values based on spontaneous and strain-induced polarization at the GaN/AlN interface [23,32,33]. Using the derived $n(T)$ and the measured zero-field $R_0(T)$ curves in Fig.1(c) we calculated the temperature dependence of the electron mobility $\mu(T)$ and present it in Fig.1(d). The Hall mobility is $\mu = 8000 \text{ cm}^2\text{V}^{-1}\text{s}^{-1}$ at $T = 3 \text{ K}$ and decreases slowly with temperature up to 100 K, then it decreases more rapidly down to $\mu = 2000 \text{ cm}^2\text{V}^{-1}\text{s}^{-1}$ at 260 K, mainly due to strong optical phonon scattering which is dominant in the high temperature region [46]. Compared to the electron mobility of 2DEGs in AlGaAs/GaAs heterostructures [7,8] where $\mu \sim 10^6\text{-}10^7 \text{ cm}^2\text{V}^{-1}\text{s}^{-1}$, our observed value is relatively low but typical for AlGaN/GaN heterostructures [32,33,47].

Figure 2(a) shows $MR(B)$ curves obtained in magnetic fields of $-12 \text{ T} \leq B \leq +12 \text{ T}$ and at $T = 3\text{K}$. At very low magnetic fields (inset of Fig.2(a)), the longitudinal resistance behavior shows a rapid decrease that can be attributed to WLs, typically observed in disordered semiconductor systems [15,16]. The MR s show a negative parabolic magnetoresistance in the range of intermediate magnetic fields as demonstrated by the inset of Fig.2(b). In higher magnetic fields, Shubnikov de Haas (SdH) quantum oscillations [19] are observed. Concurrently, at the fields where SdH oscillations emerge, the MR deviates from a parabolic magnetic field dependence (see Fig.2(b)). It is worth noting that the WL-induced MR s and SdH oscillations occur only at low temperatures and both effects gradually weaken and disappear with the increase of temperature. Meanwhile, the magnitude of the NMRs decreases gradually with increasing temperature, and eventually positive MR s emerge at high temperatures (see Fig.2(c); more data are shown in Fig.S2(a)). Similar results are obtained in CH2 of Sample W1 (Fig.S2(b)) and Sample W2.

Besides weak localizations that induce small NMRs at very weak fields with a cusp at zero field, various other mechanisms based on both quantum [24-26,31] and quasiclassical [27-29] origins have been proposed to account for the large NMRs that occur at higher magnetic fields. For example, electron–electron interactions (EEl)s were considered in understanding the NMRs in high mobility $[(0.42-5.5)\times 10^5 \text{ cm}^2\text{V}^{-1}\text{s}^{-1}]$ 2DEGs in AlGaAs/GaAs heterostructures [1,2]. The EEl)s lead to a parabolic negative magnetoresistance at $\omega_c\tau > 1$ [Refs.2,26]:

$$MR = -\frac{(\omega_c\tau)^2}{\pi k_F l} G_F(k_B T\tau/\hbar) \quad (1)$$

where $\omega_c = eB/m^*$ is the cyclotron frequency and m^* is the effective mass, k_F is the Fermi wave number and l is the mean free path. The function $G_F(x)$ has the asymptotes $G_F(x \ll 1) \approx \text{const} - \ln x$ and $G_F(x > 1) \approx (c_0/2)x^{-1/2}$, with $c_0 \approx 0.276$. Clearly, Eq.1 correctly describes the parabolic behavior in the magnetic field dependence of the observed NMRs, as presented in Fig.2(b), where $B > 1.25$ T satisfies the requirement of $\omega_c\tau > 1$ at $\mu = 8000 \text{ cm}^2\text{V}^{-1}\text{s}^{-1}$. Qualitatively, Eq.1 can also account for the decrease of the NMR's amplitude with increasing temperature, as shown in Fig.2(c).

However, the derived experimental G_F varies with $k_B T\tau/\hbar$ much slower than that predicted from theory (see Fig.S3(a)). More importantly, an essential feature of the EEI theory is that the impurities are treated as smooth random potential (remote impurities). This condition is satisfied in high-mobility GaAs structures, where doping impurities are separated from the 2DEGs by an undoped spacer and the scattering potential has a long-range character [2]. However, in AlGaN/GaN heterostructures, a random array of strong scatterers (such as interface roughness)

that give rise to predominantly large angle scattering can exist and contribute to the occurrence of large NMRs [19].

In the presence of strong scatterers, the Lorentz-Boltzmann quasiclassical model predicts that a fraction P of the electrons in the 2DEG system remains eternally in collisionless cyclotron orbits around the scatterers. Such orbiting electrons do not contribute to the conductivity σ_{xx} ; however, they give a nonzero contribution to σ_{xy} . The rest of the wandering electrons which collide with scatterers follow the conventional Drude expressions for conductivity. Taking into account the contributions of both types of electrons, the resultant longitudinal resistivity is given by [28]:

$$\rho_{xx} = \rho_0 \frac{1-P}{1+P^2/\beta^2} \quad (2)$$

where ρ_0 is the zero-field resistivity, $P = \exp(-2\pi/\beta)$, $\beta = l_{tr}/R_c$ with l_{tr} being the transport mean free path, $R_c = v_F/\omega_c$ the cyclotron radius, and v_F the Fermi velocity. As shown in Fig.S3(b), Eq.2 predicts a much stronger field dependence of the NMRs than the experimentally observed one.

In real systems, a combination of different types of disorder such as background impurities, interface roughness, and dislocations can exist. After considering memory effects in a 2DEG with a random array of strong scatterers on the background of a smooth random potential remote impurities, Mirlin et. al. also obtained a negative parabolic correction to the magnetoresistance [29]:

$$MR \approx -(\omega_c/\omega_0)^2 \quad (3)$$

where $\omega_0 = (2\pi N_s)^{1/2} v_F (2l_s/l_L)^{1/2}$, with N_s being the concentration of strong scatterers, and l_s and l_L the mean free paths due to the scattering by strong and smooth potential scatterers,

respectively.

Although Eq.3 can account for the observed parabolic relationship between the NMRs and the magnetic field as does Eq.1, this quasiclassical model predicts a temperature-independent NMR. At $T \leq 15$ K, NMRs in our samples are indeed temperature-insensitive. However, at $T > 15$ K the temperature suppresses the NMRs, as demonstrated in Fig.2(c) and Fig.S2(a). It is possible that both quantum (EEI) and quasiclassical effects contribute to the observed NMRs, resulting in the observed change of NMRs with temperature [10]. The upturn of the MRs at high magnetic fields also indicates possible contributions by Zeeman splitting that can give rise to positive MRs [2,25], which become more pronounced at higher temperatures. In fact, Cho et al. investigated NMRs of the 2DEG in an AlGaIn/GaN heterostructure and concluded that quantum contribution and quasiclassical effects co-exist, with a dominance of the latter [19]. Cho et al. used the ratio of τ_{tr}/τ_q to elucidate the type of strong scatterers that cause the quasiclassical NMRs, where τ_{tr} and τ_q are transport scattering time and the single particle relaxation time or quantum time, respectively. τ_{tr}/τ_q is close to one for alloy or phonon scattering, while it could be significantly enhanced for scattering by interface roughness. They obtained a ratio of ~ 10 and attributed the interface roughness to be the strong scatterers.

Shubnikov–de Haas (SdH) quantum oscillations contain rich information of the 2DEG, i.e., the density of the charge carriers, their effective mass and quantum scattering time. Data in Fig.2 shows pronounced SdH quantum oscillations in our sample. Figure 3(a) presents the data after subtracting the background at temperatures between 3 K to 20 K, with the fast Fourier transform (FFT) results shown in Fig.3(b). From the SdH oscillation frequency $f = 214$ T, we obtain the

2DEG density $n = 1.05 \times 10^{13} \text{ cm}^{-2}$ from the relationship of $f = hn/2e$, where h is the Planck constant, and e is electron charge. This value is consistent with the electron density derived from the Hall measurements, as presented in Fig.1(d). The SdH oscillation frequency shows no subbands, indicating that only one type of charge carrier is present in our sample, i.e., the sample is of high quality.

The SdH oscillations can be used to derive the effective mass m^* and the quantum time τ_q through the Lifshitz-Kosevich formula [19]:

$$\frac{\Delta R}{R_0} = \frac{4X}{\sinh X} \exp\left(-\frac{\pi}{\omega_c \tau_q}\right) \cos\left(\frac{2\pi^2 \hbar n}{eB}\right) \quad (4)$$

where ΔR is the SdH oscillation component of the resistance (see Fig.3(a)), $X = 2\pi^2 k_B T / \hbar \omega_c$, k_B is Boltzmann constant and \hbar is the reduced Planck constant. Since the cyclotron frequency $\omega_c = eB/m^*$, the effective mass m^* can be derived from the temperature dependence of ΔR at a fixed magnetic field. We chose ΔR_M at $B = 11.46 \text{ T}$ corresponding to the largest positive peak in the SdH oscillations and plot them in Fig.3(c). A curve fit with Eq.4 gives $m^* = 0.1975m_0$, with m_0 being the free electron mass. From the mobility μ values in Fig.1(d) and the relationship $\mu = e \tau_r / m^*$, we obtain the transport scattering time $\tau_r \approx 0.73 \text{ ps}$. For a fixed temperature, we can simplify Eq.4 to $\ln\left(\frac{\Delta R_M \sinh X}{4R_0 X}\right) \approx -\frac{\pi m^*}{Be\tau_q}$ to derive the quantum time τ_q , where ΔR_M represents the peak values at magnetic fields where $\cos\left(\frac{2\pi^2 \hbar n}{eB}\right) = 1$. Figure 3(d) presents the experimental results of $\ln\left(\frac{\Delta R_M \sinh X}{4R_0 X}\right) \sim -1/B$ for $T = 3 \text{ K}$. The slope gives a quantum time of $\tau_q = 0.078 \text{ ps}$, resulting in a ratio of $\tau_r / \tau_q \approx 9.2$.

The determined ratio of τ_r / τ_q in our sample is very close to the value of 10 obtained by Cho et al for an AlGaIn/GaN heterostructure [19]. However, the quantum time τ_q deduced from the

analysis of the SdH oscillations is much smaller than the quantum scattering time τ_{cr} determined from the width of the cyclotron resonance peak in the presence of small macroscopic inhomogeneity [48]. EEI experiments also reveal τ_{tr}/τ_q of 4~20 for long-range scattering by background impurity [2]. Thus, it is debatable if the ratio of τ_{tr}/τ_q can provide a reliable way to determine the scattering mechanism [19,48]. In order to directly uncover the scattering mechanisms responsible for the observed NMRs, we conducted electric field gating experiments to determine the mobility versus electron density relationship, which is strongly correlated with the various scattering mechanisms and can be quantitatively analyzed [32,33].

Figure 4(a) shows the dependence of sample resistances on the gate voltage V_g at $B = 0$ T and 12 T. As expected, the curve for $B = 0$ T is smooth while that for $B = 12$ T depicts oscillations due to gating-induced change in the electron density which varies the Fermi level, resulting in SdH quantum oscillations in a fixed magnetic field. In Fig.5(a) we present the relationship between the electron density determined using Hall measurements and the gate voltage. The electron density increases linearly with the gate voltage up to $V_g = 1$ V and further increases but at a slower rate beyond $V_g > 1$ V (sample W2 shows a linear relationship between the density and gate voltage at $V_g < 2$ V and a slight density decrease at $V_g > 2.3$ V, as presented in Fig.S5). This can be attributed to hole injection from the gate at high positive gating voltage [49]. By systematically measuring $R(V_g)$ curves at various magnetic fields and using the Hall electron density, we could construct an MR color map as presented in Fig.4(b). The SdH oscillations induced Landau fan diagram can be clearly seen.

Figure 4(a) also shows that the resistances do not change significantly beyond $V_g \geq -2$ V while

increasing quickly when V_g becomes more negative at $V_g < -2$ V. More importantly, the resistances at $B = 12$ T, when the SdH oscillations are neglected, can be larger than those at $B = 0$ T at very negative V_g . Inset of Fig.4(a) shows MR versus B curves at three values of V_g . Clearly, the NMRs are stronger at $V_g = 0$ V, in comparison to those at $V_g = -4$ V (in fields up to $B = 12$ T) and $V_g = 4$ V (in fields up to $B = 9$ T). It indicates that NMRs may only occur in a certain range of V_g (see Fig.S4 and Fig.S6 for similar effects in Sample W2). This can be further demonstrated by the MR versus V_g curves for various magnetic fields in Fig.5(b), where each curve shows a maximum in the amplitude of NMRs, though the corresponding V_g point shifts to more positive values with increasing magnetic field. That is, the amplitude of NMRs depends on the electron density. A more complete picture on the effects of electron density on the MR can be seen from the color map in Fig.4(b), which shows more pronounced NMRs in the intermediate range of the electron density, i.e., $0.6 \times 10^{13} \text{ cm}^{-2} < n < 1.1 \times 10^{13} \text{ cm}^{-2}$.

As pointed out above, it is the mobility versus density relationship rather the density itself that can provide information on the scattering mechanisms. Figure 5(a) presents the mobilities obtained at various gate voltages. The $\mu(V_g)$ curve exhibits a bell shape. The mobility increases rapidly with V_g first, reaches a maximal value of $12186 \text{ cm}^2\text{V}^{-1}\text{s}^{-1}$ at $V_g = -2.8$ V and then decreases slowly with a further increase in V_g .

As shown in Fig.5(a), the electron density n does not follow a linear dependence on the gate voltage at high positive V_g . We plot the experimental $\mu(n)$ data in Fig.6. Theoretically, the relationship between mobility and density is determined by the types of possibly co-existing scatterers such as background impurities, interface roughness, dislocations, and alloy disorder.

Their scattering contributions are independent of each other and the total mobility can be calculated according to Matheissen's rule by combining different scattering mechanisms [35,46]. Experimentally, the density dependence of the electron mobility in AlGaIn/GaN heterostructures has been systematically studied and found to follow the theory very well [33]. Details of the calculations, including the relevant equations and parameters are presented in the supplement [45]. Figure 6 shows a comparison of our experimental data with the calculated $\mu(n)$ curve as well as the individual contributions of background impurities, interface roughness, dislocations and alloy disorder. For simplicity we did not include the contribution from phonon scattering that is negligible at low temperatures. The results show that at low densities the electron scattering due to background impurity and dislocations limit the electron mobility, which becomes higher with increasing density. The downturn of the $\mu(n)$ curve at high electron densities is an indication of a cross-over to scattering by interface roughness, which is more than two orders of magnitude stronger than alloy scattering. The negligible influence of alloy scattering on total mobility is expected due to the intentionally introduced AlN barrier [25,44]. Together with the results in Fig.5, which shows that NMRs occur in the right side of the bell-shaped $\mu(V_g)$ curve and tend to vanish quickly in the left side, we can conclude that interface roughness is the key contributor to the NMRs observed in our samples.

As discussed above, strong scatterers alone could only induce NMR behavior described by Lorentz gas model Eq.2. The vanishing of NMRs in the left side of the bell-shaped $\mu(V_g)$ curve in Fig.5 where scattering of smooth random potential dominates can also exclude the EEI mechanism that gives Eq.1 as the origin of the observed NMRs. On the other hand, Eq.3 can correctly explain

the parabolic behavior as shown in Fig.2. Fig.6 also shows the presence of both strong scatterers and smooth random potential. Thus, we can safely attribute the observed NMRs to memory effects. This is in fact consistent with the results in Figs.4(b), Fig.5(b) and Fig.6, which reveal that NMRs are more pronounced when the scatterings from interface roughness and background impurity are comparable. They diminish quickly when the contribution of interface roughness is weaker than that from dislocations. On the other hand, the amplitude of the NMR also becomes smaller when the effect of background impurity is reduced at high electron density.

IV. CONCLUSION

In summary, we investigated the magnetoresistance behavior of 2DEGs in AlGaIn/GaN heterostructures. Large NMRs were observed in a wide range of temperature. Analysis of the magnetic field and temperature dependences of the NMRs as well as the ratio of transport scattering time and quantum time suggest that the observed NMRs most likely originate from memory effects, with interface roughness to be the strong scatterers. We also conducted electric field gating experiments to obtain the electron mobility and density relationship that helps to further uncover the underlying scattering sources in the sample. The results confirmed the crucial role of interface roughness scattering in the occurrence of NMRs and also demonstrated that electric field gating can be a useful means in uncovering the various mechanisms for NMRs.

ACKNOWLEDGMENTS

This work is supported by the National Key R&D Program of China (2018YFA0209002), the National Natural Science Foundation of China (61771235, 61971464, 61727805, 11961141002,

61974113, 62074077, 61921005, 61674080, and 61974060), Jiangsu Excellent Young Scholar Program (BK20200008) and Jiangsu Shuangchuang Program. W. K. Kwok is supported by the U.S. Department of Energy, Office of Science, Basic Energy Sciences, Materials Sciences and Engineering. Z.-L.X. acknowledges supports by the National Science Foundation under Grant No. DMR-1901843.

*Correspondence to: xiao@anl.gov; yongleiwang@nju.edu.cn; xllu@xidian.edu.cn

References

- [1] M.A. Paalanen, D.C. Tsui, and J. C.M. Hwang, Phys. Rev. Lett. **51**, 2226 (1983).
- [2] L. Li, Y. Y. Proskuryakov, A. K. Savchenko, E. H. Linfield, and D. A. Ritchie, Phys. Rev. Lett. **90**, 076802 (2003).
- [3] L. Bockhorn, P. Barthold, D. Schuh, W. Wegscheider, and R. J. Haug, Phys. Rev. B **83**, 113301 (2011).
- [4] A. T. Hatke, M. A. Zudov, J. L. Reno, L. N. Pfeiffer, and K. W. West, Phys. Rev. B **85**, 081304(R) (2012).
- [5] R. G. Mani, A. Kriisa, and W. Wegscheider, Sci. Rep. **3**, 2747 (2013).
- [6] L. Bockhorn, I. V. Gornyi, D. Schuh, C. Reichl, W. Wegscheider, and R. J. Haug, Phys. Rev. B **90**, 165434 (2014).
- [7] Q. Shi, M. A. Zudov, L. N. Pfeiffer, and K. W. West, Phys. Rev. B **90**, 201301(R) (2014).

- [8] Q. Shi, P. D. Martin, Q. A. Ebner, M. A. Zudov, L. N. Pfeiffer, and K.W. West, Phys. Rev. B **89**, 201301 (2014).
- [9] J. Iñarrea, L. Bockhorn, and R. J. Haug, Europhys. Lett. **115**, 17005 (2016).
- [10] J. Kanter, S. Vitkalov, and A. A. Bykov, Phys. Rev. B **97**, 205440 (2018).
- [11] N. H. Siboni, J. Schluck, K. Pierz, H.W. Schumacher, D. Kazazis, J. Horbach, and T. Heinzl, Phys. Rev. Lett. **120**, 056601 (2018).
- [12] J. Schluck, M. Hund, T. Heckenthaler, and T. Heinzl, N. H. Siboni and J. Horbach, K. Pierz, H. W. Schumacher, D. Kazazis, U. Gennser, and D. Mailly, Phys. Rev. B **97**, 115301 (2018).
- [13] R. L. Samaraweera, H.-C. Liu, B. Gunawardana, A. Kriisa, C. Reichl, W. Wegscheider, and R. G. Mani, Sci. Rep. **8**, 10061 (2018).
- [14] R. L. Samaraweera, B. Gunawardana, T. R. Nanayakkara, R. C. Munasinghe, A. Kriisa, C. Reichl, W. Wegscheider, and R. G. Mani, Sci. Rep. **10**, 781 (2020).
- [15] A. Buyanov, J. Bergman, J. Sandberg, B. Sernelius, P. Holtz, B. Monemar, H. Amano, and I. Akasaki, Phys. Rev. B **58**, 1442 (1998).
- [16] A. V. Buyanov, J. A. Sandberg, B. E. Sernelius, P. O. Holtz, J. P. Bergman, B. Monemar, H. Amano, and I. Akasaki, J. Cryst. Growth **189/190**, 758 (1998).
- [17] J. Antoszewski, M. Gracey, J. M. Dell, L. Faraone, T. A. Fisher, G. Parish, Y.-F. Wu, and U. K. Mishra, J. Appl. Phys. **87**, 3900 (2000).

- [18] A. F. Braña, C. Diaz-Paniagua, F. Batallan, J. A. Garrido, E. Muñoz, and F. Omnes, *J. Appl. Phys.* **88**, 932 (2000).
- [19] H. I. Cho, G. M. Gusev, Z. D. Kvon, V. T. Renard, J. H. Lee, and J. C. Portal, *Phys. Rev. B* **71**, 245323 (2005).
- [20] J. Xu, M. K. Ma, M. Sultanov, Z. -L. Xiao, Y. -L. Wang, D. Jin, Y. -Y. Lyu, W. Zhang, L. N. Pfeiffer, K. W. West, K. W. Baldwin, M. Shayegan, and W. -K. Kwok, *Nat. Commun.* **10**, 287 (2019).
- [21] Y.-Y. Lyu, X. -J. Zhou, Z. -L. Xiao, R. Fotovat, J. Xu, G. Basnet, Y. -L. Wang, D. Jin, R. Divan, H. -B. Wang, and W. -K. Kwok, *Phys. Rev. B* **103**, 035422 (2021)
- [22] M. K. Mishra, R. K. Sharma, R Tyagi, R Manchanda, A. K. Pandey, O. P. Thakur, and R Muralidharan, *Mater. Res. Express* **3**, 045902 (2016).
- [23] K. H. Gao, X. R. Ma, D. B. Zhou, S. Li, Z. Q. Li, T. Lin, X. H. Zhang, and W. Z. Zhou, *Superlattices and Microstructures* **135**, 106262 (2019).
- [24] B. L. Altshuler, D. Khmel'nitski, A. I. Larkin, and P. A. Lee, *Phys. Rev. B* **22**, 5142 (1980).
- [25] B. L. Altshuler and A. G. Aronov, *Electron-Electron Interaction in Disordered Systems*, edited by A.L. Efros and M. Pollak (North-Holland, Amsterdam, 1985).
- [26] I. V. Gornyi and A. D. Mirlin, *Phys. Rev. Lett.* **90**, 076801 (2003).
- [27] A. Dmitriev, M. Dyakonov, and R. Jullien, *Phys. Rev. Lett.* **89**, 266804 (2002).
- [28] A. Dmitriev, M. Dyakonov, and R. Jullien, *Phys. Rev. B* **64**, 233321 (2001).
- [29] A. D. Mirlin, D. G. Polyakov, F. Evers, and P. Wölfle, *Phys. Rev. Lett.* **87**, 126805 (2001).

- [30] V. K. Dugaev, M. Inglot, E. Y. Sherman, J. Berakdar, and J. Barnas, *Phys. Rev. Lett.* **109**, 206601 (2012).
- [31] P. S. Alekseev, *Phys. Rev. Lett.* **117**, 166601 (2016).
- [32] J. L. Farvacque and Z. Bougrioua, *Phys. Rev. B* **68**, 035335 (2003).
- [33] P. Lorenzini, Z. Bougrioua, A. Tiberj, R. Tauk, M. Azize, M. Sakowicz, K. Karpierz, and W. Knap, *Appl. Phys. Lett.* **87**, 232107 (2005).
- [34] D. Laroche, S. Das Sarma, G. Gervais, M. P. Lilly, and J. L. Reno, *Appl. Phys. Lett.* **96**, 162112 (2010).
- [35] B. Shojaei, A. C. C. Drachmann, M. Pendharkar, D. J. Pennachio, M. P. Echlin, P. G. Callahan, S. Kraemer, T. M. Pollock, C. M. Marcus, and C. J. Palmstrøm, *Phys. Rev. B* **94**, 245306 (2016).
- [36] Y. F. Wu, D. Kapolnek, J. P. Ibbetson, P. Parikh, B. P. Keller, and U. K. Mishra, *IEEE Trans. Electron Devices* **48**, 586 (2001).
- [37] R. S. Pengelly, S. M. Wood, J. W. Milligan, S. T. Sheppard, and W. L. Pribble, *IEEE Trans. Microwave Theory Technol.* **60**, 1764 (2012).
- [38] H. Otake, K. Chikamatsu, A. Yamaguchi, T. Fujishima, and H. Ohta, *Appl. Phys. Express* **1**, 011105 (2008).
- [39] B. Rau, P. Waltereit, O. Brandt, M. Ramsteiner, K. H. Ploog, J. Puls, and F. Henneberger, *Appl. Phys. Lett.* **77**, 3343 (2000).

- [40] E. Kuokstis, C. Q. Chen, M. E. Gaevski, W. H. Sun, J. W. Yang, G. Simin, M. Asif Khan, H. P. Maruska, D. W. Hill, M. C. Chou, J. J. Gallagher, and B. Chai, *Appl. Phys. Lett.* **81**, 4130 (2002).
- [41] O. Ambacher, J. Smart, J. R. Shealy, N. G. Weimann, K. Chu, M. Murphy, W. J. Schaff, and L. F. Eastman, *J. Appl. Phys.* **85**, 3222 (1999).
- [42] R. K. Jana and D. Jena, *Appl. Phys. Lett.* **99**, 012104 (2011).
- [43] Q. Li, J. Zhang, L. Meng, J. Chong, and X. Hou, *J. Nanomater.* **2015**, 903098 (2015).
- [44] L. Hsu and W. Walukiewicz, *J. Appl. Phys.* **89**, 1783 (2001).
- [45] See Supplemental Material at [URL will be inserted by publisher] for the calculation of mobility versus density relationship, a comparison of the temperature dependence of the electron density, mobility, and mean free path as well as the electron mobility versus density relationship from CH1 and CH2 of Sample W1, and for additional data from CH2 of Sample W1 and Sample W2.
- [46] D. Jena, Y. Smorchkova, C. Elsass, A. C. Gossard, and U. K. Mishra: Electron transport and intrinsic mobility limits in two-dimensional electron gases of III–V nitride heterostructures. arXiv:cond-mat/0103461 (2001).
- [47] N. Tang, B. Shen, K. Han, F. C. Lu, Z. X. Qin and G. Y. Zhang, *Phys. Rev. B* **79**, 073304 (2009).
- [48] S. Syed, M. J. Manfra, Y. J. Wang, R. J. Molnar, and H. L. Stormer, *Appl. Phys. Lett.* **84**, 1507 (2004).

[49] M. Meneghini, M. Scamperle, M. Pavesi, M. Manfredi, T. Ueda, H. Ishida, T. Tanaka, D. Ueda, G. Meneghesso, and E. Zanoni, *Appl. Phys. Lett.* **97**, 033506 (2010).

Figure captions

Fig.1. (a) Schematic (not-to-scale) of the layer structuring of the AlGaIn/GaN heterostructure. (b) Micrograph and enlarged view of the sample in Hall bar geometry with width of $L_y = 200$ μm and voltage lead distance of $L_x = 250$ μm . CH1 And CH2 in the enlarged view denote the measured Hall bar sections. Each section has four voltage contacts, with one pair in the longitudinal direction for measuring R_{xx} and one pair in the transverse direction for measuring R_{xy} . (c) Temperature dependence of the sample resistance in the absence of a magnetic field and the Hall resistance at $B = 9$ T. Inset shows the linear field dependence of the Hall resistances at the lowest ($T = 3$ K) and highest ($T = 260$ K) experimental temperatures. (d) Temperature dependence of the electron density n and mobility μ derived from data in (c).

Fig.2. (a) Magnetoresistance MR at $T = 3$ K. The inset is an expanded view to show the weak localization induced cusp at zero-field. (b) Data in (a) plotted as MR versus B^2 to show the parabolic field dependence. The main panel shows the linear section while the inset present the complete set of data. (c) Magnetoresistances MRs obtained at various temperatures. The magnetic field is applied perpendicular to the 2DEG.

Fig.3. (a) Magnetic field dependence of the resistance components ΔR induced by Shubnikov–de Haas (SdH) quantum oscillations at various temperatures. (b) Fast Fourier transform (FFT)

spectra of the data in (a). (c) Temperature dependence of ΔR_M at $B = 11.46$ T (positive maxima in the SdH oscillations). Circles are experimental data and the line is a fit to Eq.4 to derive the effective mass m^* . (d) Magnetic field dependence of peak values ΔR_M in the SdH oscillations at $T = 3$ K. Circles are experimental data and the line is a fit to derive the quantum time from Eq.4.

Fig.4. (a) Gate voltage dependence of the sample resistance at $B = 0$ T and 12 T. The inset presents MR versus B curves obtained at various gate voltages. (b) Color map of the field and electron density dependences of the magnetoresistance MR . It is constructed by taking $R \sim Vg$ curves at magnetic fields from 0 T to 4.5 T in intervals of 0.5 T and from 4.5 T to 12 T in intervals of 0.25 T. The data were taken at $T = 3$ K.

Fig.5. Gate voltage dependence of the electron mobility and density (a) and magnetoresistance MR (b). The electron density is calculated from the measured Hall resistance. The mobility is derived from the measured zero-field resistance and the calculated Hall electron density. The data were taken at $T = 3$ K.

Fig.6. Comparison of the experimental and theoretical relationships between the electron mobility and density. Symbols are for experimental data and curves are calculated (Equations and discussions are presented in the supplement).

Figure 1

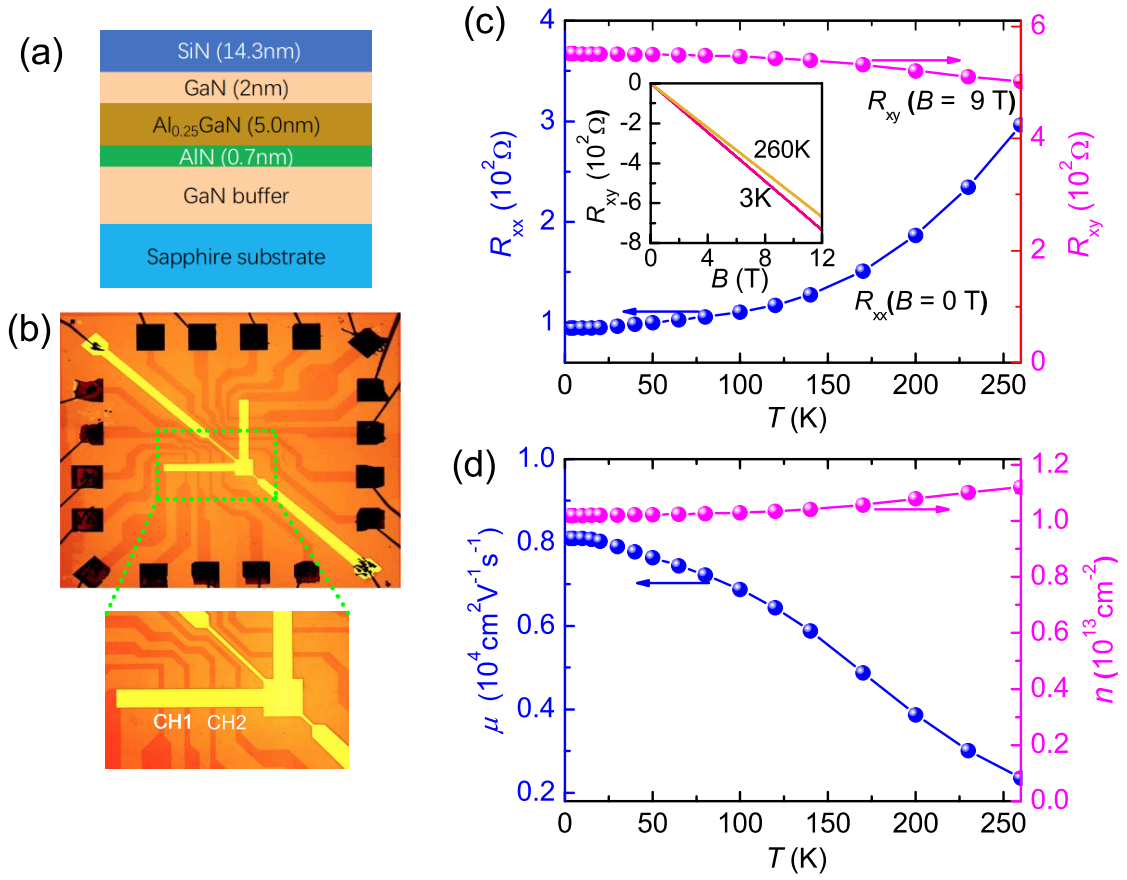


Figure 2

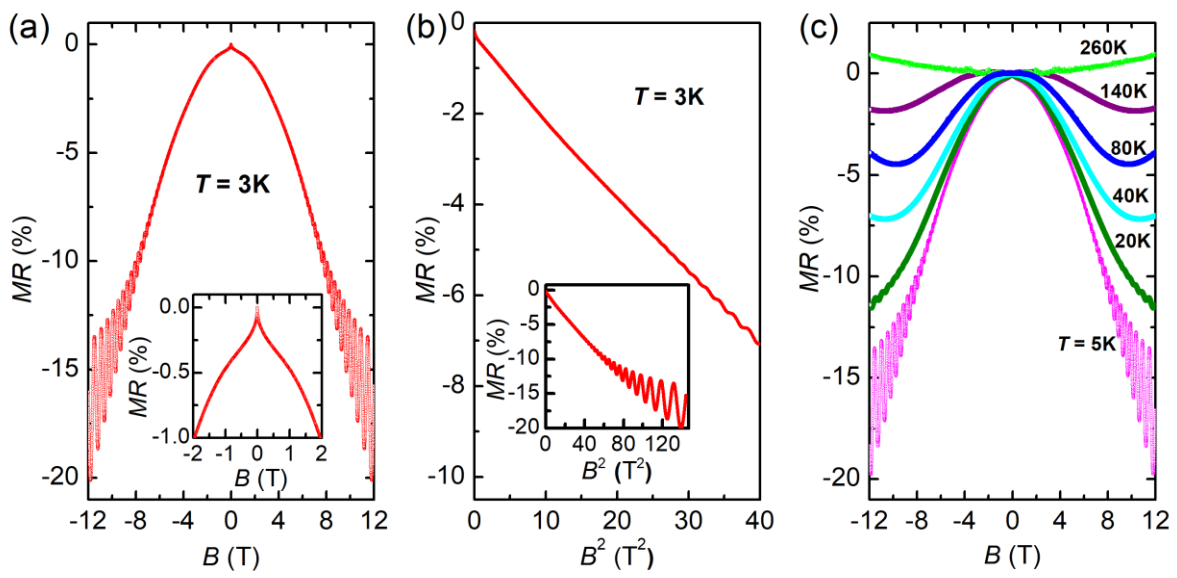


Figure 3

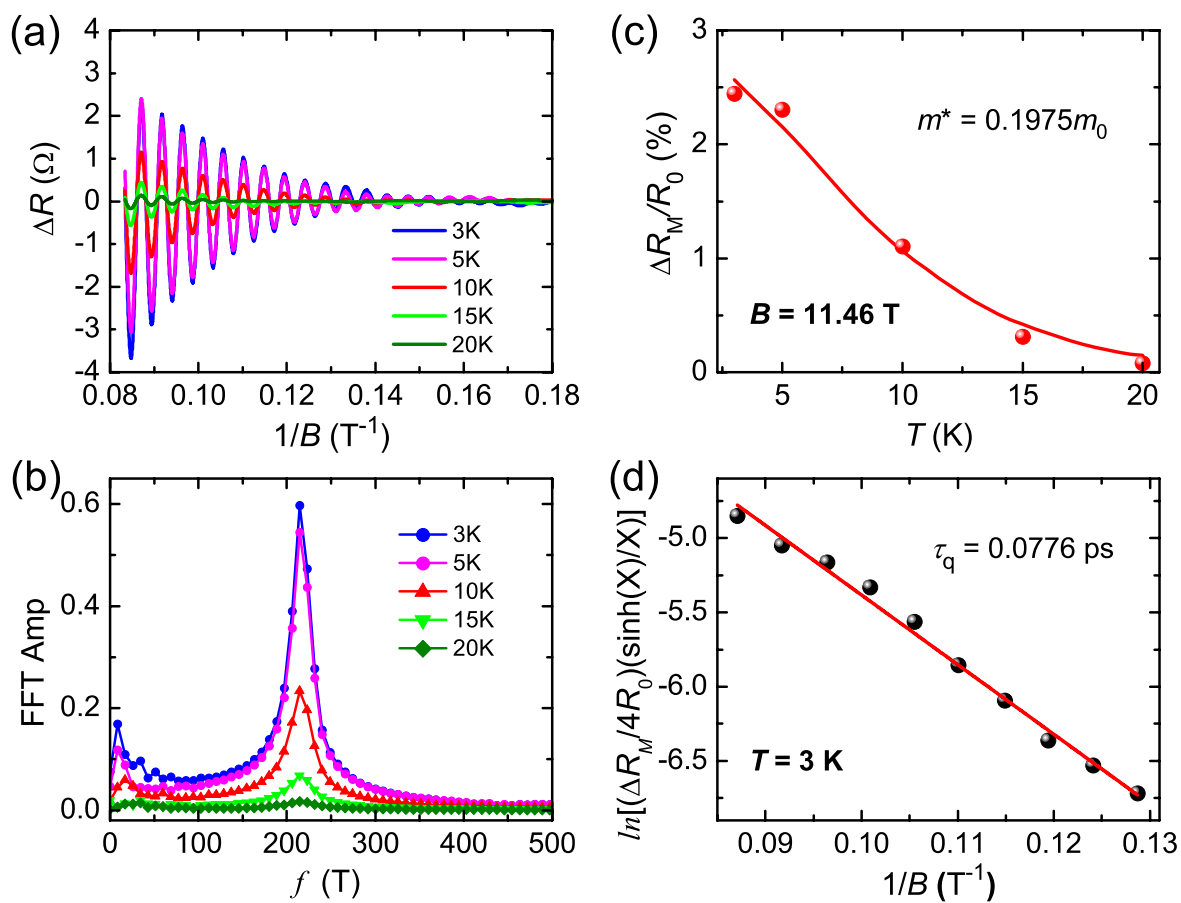


Figure 4

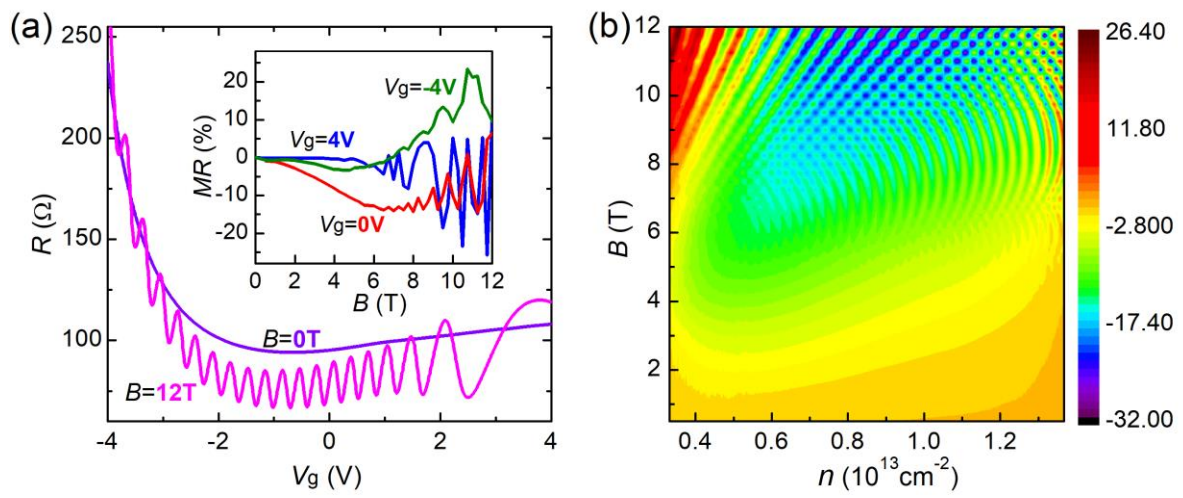


Figure 5

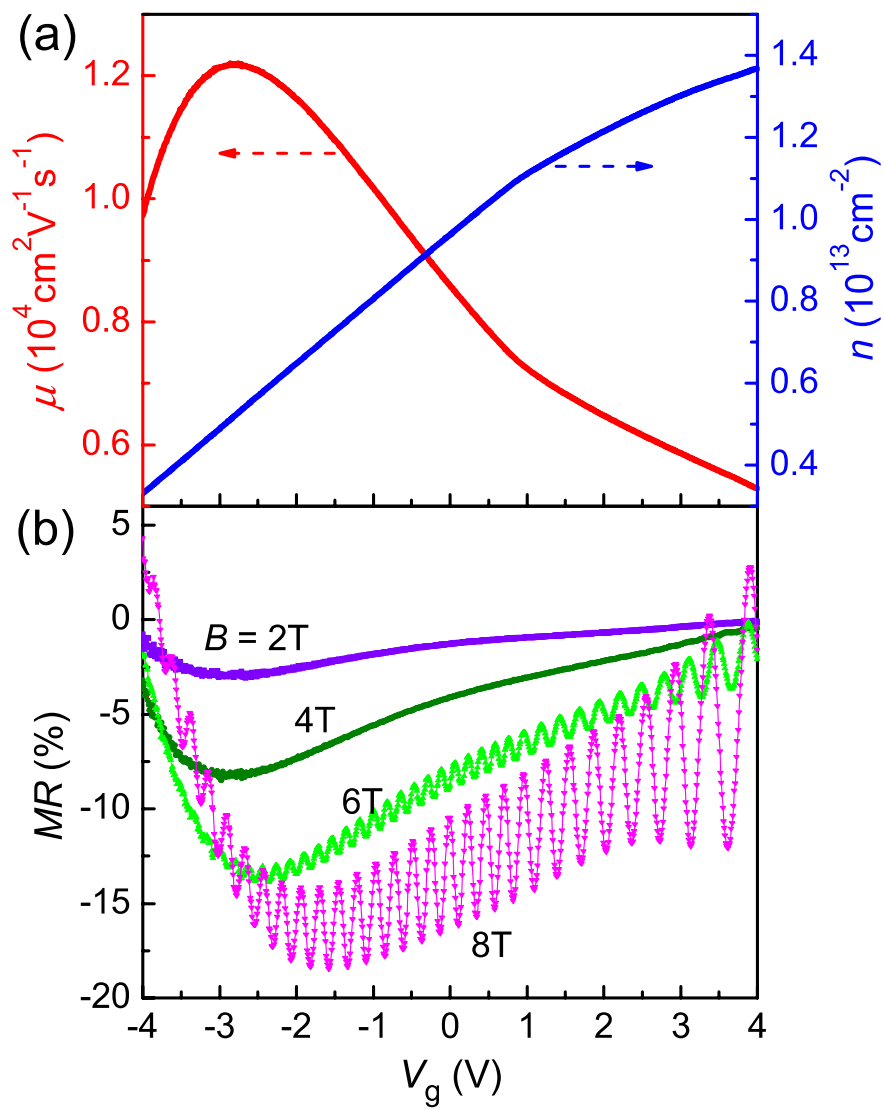


Figure 6

